Expressions for local contributions to the surface tension from the virial route

A. Ghoufi,[1] F. Goujon,[2] V. Lachet,[1] and P. Malfreyt[2,*]
[1]*IFP, 1–4 avenue de Bois Préau, 92852 Rueil-Malmaison Cedex, France*
[2]*Laboratoire de Thermodynamique des Solutions et des Polymères, UMR 6003 CNRS, Université Blaise Pascal, 63177 Aubière Cedex, France*

(Received 30 October 2007; revised manuscript received 5 January 2008; published 3 March 2008)

The expression of the surface tension using the virial route has been reinvestigated in order to establish a local version of the surface tension and of its long-range corrections. In fact, giving a local surface tension is very important for the simulation from a methodological viewpoint. It is also of basic interest to associate the profile of the intrinsic part of the surface tension with that of the long-range corrections to make the surface tension calculation consistent between the different approaches that can be used. Working expressions for two-phase systems interacting through dispersion-repulsion (Lennard-Jones) and Coulombic (Ewald summation) interactions are proposed. Different operational expressions of the surface tension are compared in the cases of *n*-pentane, carbon dioxide, and water liquid-vapor equilibria for which the orders of magnitude between the electrostatic and dispersion forces are different.

DOI: 10.1103/PhysRevE.77.031601 PACS number(s): 68.03.Cd

I. INTRODUCTION

Direct molecular simulation of two-phase systems allows the calculation of the surface tension coupled with a microscopic description of the interfacial region. The difficulties of this method are directly related to the nature of the system, i.e., the nonuniformity of the local density along the direction normal to the surface. Due to this heterogeneity, care must be taken when dealing with the truncation procedures involved in the calculation of the potential energy and corresponding force [1,2], the long-range corrections to apply to the macroscopic properties [3–8], and the definition of local thermodynamic functions such as the local pressure tensor or the energy density [9].

In the case of a planar liquid-vapor interface lying in the x,y plane, the density gradient occurs in the z direction normal to the surface. It is then of fundamental interest to check the behavior of some local thermodynamic properties along this direction. The surface tension γ can be expressed as $\int_{-\infty}^{\infty}[p_N(z)-p_T(z)]dz$ where $p_N(z)$ and $p_T(z)$ are local values of the normal and tangential components of the pressure tensor, respectively. Expressing the surface tension as a function of the local components of the pressure allows use of a local $\gamma(z)$ defined as $\int_{-\infty}^{z}[p_N(z)-p_T(z)]dz$. The use of $\gamma(z)$ is a key element to check the validity of the calculation concerning the stabilization of the interfaces, the independence between the two interfaces, and the constancy of $\gamma(z)$ in the bulk phases. We note that there are many ways of expressing the local components of the pressure, which depend on the contour joining two interacting molecules. Irving and Kirkwood (IK) [10–12] use a straight line to join the two particles. This choice is the most natural and the one generally made. Harasima's expression [13] leads to a different expression for the tangential component of the pressure tensor. The profile of $p_T(z)$ calculated using the IK definition shows small positive peaks [11] on the gas side of the liquid-vapor interface that are missing in Harasima's expression. This highlights the fact that the way of specifying which intermolecular forces contribute to the stress across dA can lead to slight differences in the local values of the components of the pressure tensor between the different possible contours. This problem was analyzed in detail elsewhere [14]: the authors concluded that there are many ways of writing the local components of the pressure tensor. Nevertheless, the scalar value of surface tension is invariant to the choice of the pressure tensor. Until recently, only the method of Irving and Kirkwood was designed to provide a profile of the surface tension.

Figure 1(a) shows the accumulated average values of the surface tension of water calculated with two different simulation times of 2 and 4 ns using molecular dynamics simulations. We report this property in Fig. 1(a) as a function of the number of configurations saved during the simulation. Let us recall that the number of saved configurations is the same for the two total simulation times. Figure 1(b) shows the $p_N(z)-p_T(z)$ profiles whereas Fig. 1(c) displays the profiles of the integral of $p_N(z)-p_T(z)$. Interestingly, we observe significant differences in the local surface tension profiles of Fig. 1(c), whereas the scalar average value of γ does not show time dependence. Figure 1(c) shows that the two interfaces are not completely stabilized with a liquid region contributing to the surface tension in the case of a simulation of 2 ns whereas the simulation of 4 ns leads to a flat profile of $\gamma(z_k)$ in the liquid region, indicating that only the two interfaces contribute to the surface tension. This example aimed to establish the importance of the calculation of the surface tension profile along the direction normal to the surface. This is an essential check for the methodology of a molecular simulation of a two-phase system and an important route to finding the surface tension of interfaces.

Other routes can be used to calculate the surface tensions. The most general working expression uses macroscopic normal and tangential pressures which can be related to the derivative of the pair potential. The final form was obtained by Kirkwood and Buff (KB) [15–18] and is referred to as γ_{KB}

*Patrice.MALFREYT@univ-bpclermont.fr

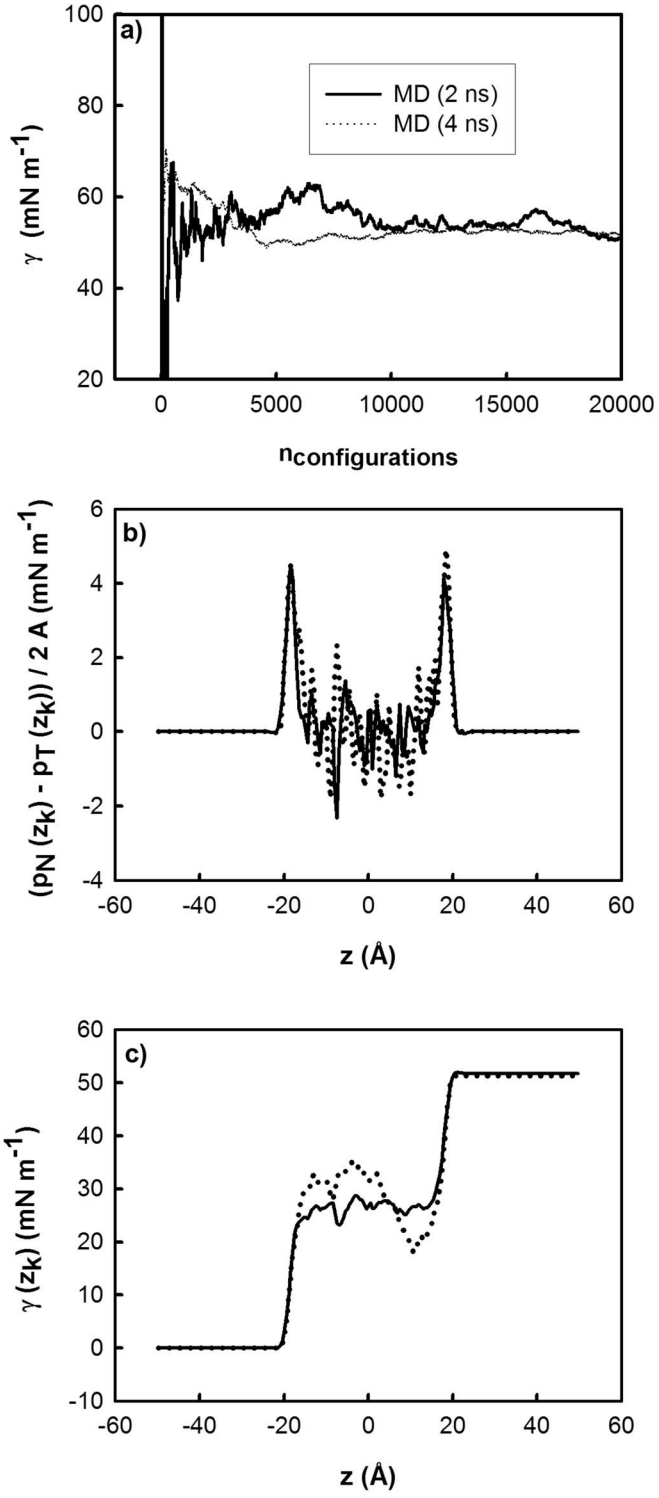

FIG. 1. (a) Accumulated time average values of the surface tension of the liquid-vapor interface for the TIP4P water model at a temperature of 400 K calculated over a simulation time of 2 (solid line) and 4 ns (dotted line). (b) $p_N(z_k)-p_T(z_k)$ profile as a function of z_k. (c) Integral of $p_N(z_k)-p_T(z_k)$ calculated from the two simulation times as indicated in the legend of (a).

throughout this paper. Using this expression, we obtain a macroscopic scalar surface tension which compares very well with that of the IK definition, even if the operational expressions of these definitions result from different approximations. Recently, the "test-area" [19] (TA) method based upon the perturbation formalism was proposed for the calculation of the surface tension. This method uses the perturbation formalism and takes advantage of expressing the surface tension as a difference of energy between a reference state and a perturbed state characterized by an infinitesimal increase or decrease of the surface. However, the aspect of the local surface tension was missing within the virial (KB) and test-area (TA) methods. This led us to establish the local expression of the surface tension calculated from the test-area approach in a recent work [20] and to propose here the local version of the surface tension resulting from the virial route.

It is also of basic interest to note that the most commonly used (KB and IK) methods for the surface tension calculation use the derivative of the potential energy in their operational expressions, whereas the TA method uses only the configurational energy. This may lead to significant discrepancies between the different methods when truncated potential energy and forces are used. In fact, the problems associated with the truncation procedures were reported in previous papers [1,2,20]. We established that the value of the intrinsic part of the surface tension was consistent within the different definitions if the discontinuities in the potential and force equations were removed. Additionally, the use of truncated potential requires addition of long-range corrections (LRCs) to the thermodynamic properties, and an inconsistent treatment of the long-range corrections to the surface tension can lead to conflicting results between the different methods. It is also essential to associate an appropriate expression of the tail correction with that of the intrinsic part of the surface tension. A certain number of expressions for calculating the LRC contributions of the surface tensions have been developed [3–8]. Some of them [5–8] express the LRC contributions of the surface along the direction perpendicular to the interface. Our conclusions from a previous work [20] showed that the different methods (IK, TA, and KB) matched very well as long as appropriate LRC contributions were included in the calculation. In that work, the operational expression of the LRC profile [20] of the surface tension within the TA approach was also proposed.

Before giving the different steps leading to the operational expressions of the local surface tension for a planar surface and of its long-range corrections within the virial route, we need to recall some fundamental expressions for the perturbation formalism. The most popular methods for the calculation of the free energy difference are the free energy perturbation (FEP) [21–23] and the thermodynamic integration (TI) [24–26] methods. Both methods use a master equation derived from classical statistical mechanics to give the working expression for the free energy calculation. FEP relies on the master equation

$$\Delta F = F^1 - F^0 = -k_B T \sum_{\lambda=0}^{\lambda=1} \ln \left\langle \exp\left(-\frac{(U^{(\lambda+\Delta\lambda)} - U^{(\lambda)})}{k_B T} \right) \right\rangle_{\lambda} \tag{1}$$

where T is the temperature, k_B is the Boltzmann constant. and λ is defined as a coupling parameter [24] going from 0 to

1. $U^{(\lambda+\Delta\lambda)}-U^{(\lambda)}$ is the energy difference between states $\lambda+\Delta\lambda$ and λ and $\langle\cdots\rangle_\lambda$ indicates an ensemble average at state λ. The second method, TI, uses the following master equation:

$$\Delta F=\int_0^1\left(\frac{\partial F_\lambda}{\partial\lambda}\right)d\lambda=\int_0^1\left\langle\frac{\partial U}{\partial\lambda}\right\rangle_\lambda d\lambda, \tag{2}$$

where F_λ is the free energy of the state λ. While FEP has been more widely applied for the free energy calculations than TI, TI has some advantages by not using the logarithm of the average of an exponential function as in FEP. By analogy, we observe that the TA method is based upon the free energy perturbation. We will show that the surface tension resulting from the virial route and expressed as the derivative of the potential energy with respect to the surface can also be considered throughout the TI formalism.

The local expression of the surface tension derived from the virial route is referred to as the KBZ expression where Z indicates the direction of the density gradient. The resulting value of surface tension calculated from the KBZ expression is discussed along with those calculated from the TA, IK, and KB approaches. These expressions are given within the framework of a planar interface of a two-phase system interacting through 6-12 Lennard-Jones interactions and electrostatic contributions. The case of nonplanar surfaces is not investigated here. The TA and KBZ approaches can be extended to other types of interfaces. For example, in a cylindrical interface parallel to the z direction, the local thermodynamic properties will depend on R, which is defined as $\sqrt{x^2+y^2}$ within a cylindrical coordinate system. The surface area expressed as $2\pi RL_z$ is no longer a constant and the operational expressions of the surface tension and of its long-range corrections within the TA and KBZ approaches must be rewritten within this cylindrical coordinate system. Further details concerning the calculation of the surface tension in curved interfaces may be found elsewhere [27–29]. All the expressions developed in this paper are written for planar surfaces.

The paper is arranged as follows: In Sec. II, we reinvestigate the different steps leading to the operational expressions of γ using the virial route with Lennard-Jones and electrostatic contributions [30,31]. We compare in Sec. III the different operational expressions (TA, KBZ, IK, and KB) in systems involving different orders of magnitude for the dispersion-repulsion and electrostatic interactions (n-pentane, CO_2, and H_2O). In Sec. IV, we draw the main conclusions from this work.

II. SURFACE TENSION CALCULATION

A. Volume perturbation

In the constant-NVT ensemble, the surface tension γ is defined as the derivative of the Helmholtz energy with respect to the interfacial area A:

$$\gamma=\left(\frac{\partial F}{\partial A}\right)_{N,V,T}=\lim_{\Delta A\to 0}\left(\frac{\Delta F}{\Delta A}\right)_{N,V,T}. \tag{3}$$

The surface tension given in Eq. (3) represents the change in free energy for an infinitesimal change in the area. This infinitesimal change in the area can be performed throughout a perturbation process in which the box dimensions are virtually changed by a small quantity ϵ such as $\epsilon\ll 1$. These transformations conserve the volume of the box in the perturbed state. Let us consider a system with L_x, L_y, and L_z as the box dimensions. $V=L_xL_yL_z$ and $A=2L_xL_y$ are the volume and the overall interfacial area of the system, respectively. The factor 2 is introduced in the interfacial area because two interfaces are considered in the system due to the use of periodic boundary conditions. It is then possible to express the surface tension as a ratio of partition functions between the perturbed and reference states as in Eq. (4). This leads to Eq. (5), where $U^{(0)}(\mathbf{r}^N)$ and $U^{(1)}(\mathbf{r}'^N)$ are the configurational energies of the systems with area $A^{(0)}$ and configurational space $\mathbf{r}^N$, and with area $A^{(1)}$ and configurational space $\mathbf{r}'^N$, respectively:

$$\begin{aligned}\gamma&=\left(\frac{\partial F}{\partial A}\right)_{N,V,T}\\&=\lim_{\epsilon\to 0}\frac{F(N,V,T,A^{(1)})-F(N,V,T,A^{(0)})}{\Delta A}\\&=\lim_{\epsilon\to 0}-\frac{k_BT}{\Delta A}\ln\frac{Q_{NVT}^{(1)}}{Q_{NVT}^{(0)}}\end{aligned} \tag{4}$$

$$=\lim_{\epsilon\to 0}-\frac{k_BT}{\Delta A}\ln\left\langle\exp\left(-\frac{U^{(1)}(\mathbf{r}'^N)-U^{(0)}(\mathbf{r}^N)}{k_BT}\right)\right\rangle_0 \tag{5}$$

where $\Delta A=2L_xL_y\epsilon$ is an infinitesimal variation of the interfacial area. $\langle\cdots\rangle_0$ denotes the canonical average over the reference system. The expression given in Eq. (5) has been established by Gloor *et al.* [19] and has led to a novel approach called the test-area technique. Let us recall that the formalism used to establish this working expression is that used for the calculation of the free energy difference in the FEP approach.

Let us apply the formalism used in the TI approach to the calculation of γ. From the derivation of Eq. (6) with respect to the surface area, we obtain an expression of γ depending on the derivative of the partition function with respect to A according to Eq. (7):

$$F=-k_BT\ln Q_{NVT}, \tag{6}$$

$$\gamma=\left(\frac{\partial F}{\partial A}\right)_{N,V,T}=-\frac{k_BT}{Q_{NVT}}\left(\frac{\partial Q_{NVT}}{\partial A}\right)_{N,V,T}, \tag{7}$$

where the partition function Q_{NVT} is expressed as

$$Q_{NVT} = \frac{1}{\Lambda^{3N} N!} \int d\mathbf{r}^N \exp\left(- \frac{U(\mathbf{r}^N)}{k_B T} \right). \tag{8}$$

Λ denotes the de Broglie thermal wavelength. Differentiating Eq. (8) with respect to A gives the following expression:

$$\frac{\partial Q_{NVT}}{\partial A} = - \frac{1}{\Lambda^{3N} N!} \int d\mathbf{r}^N \frac{1}{k_B T} \frac{\partial U(\mathbf{r}^N)}{\partial A} \exp\left(- \frac{U(\mathbf{r}^N)}{k_B T} \right). \tag{9}$$

Using the canonical ensemble average, the surface tension γ, expressed as

$$\gamma = - k_B T \frac{\left[- \frac{1}{\Lambda^{3N} N!} \int d\mathbf{r}^N \frac{1}{k_B T} \frac{\partial U(\mathbf{r}^N)}{\partial A} \exp\left(- \frac{U(\mathbf{r}^N)}{k_B T} \right) \right]}{\frac{1}{\Lambda^{3N} N!} \int d\mathbf{r}^N \exp\left(- \frac{U(\mathbf{r}^N)}{k_B T} \right)}, \tag{10}$$

leads to the following operational expression of Eq. (11):

$$\gamma = \left\langle \frac{\partial U(\mathbf{r}^N)}{\partial A} \right\rangle_0. \tag{11}$$

In a first step, the term $\partial U(\mathbf{r}^N)/\partial A$ can be calculated using a second-order finite difference method. This gives the following expression for γ:

$$\gamma_{\mathrm{TA2}} = \left\langle \frac{\partial U(\mathbf{r}^N)}{\partial A} \right\rangle_0 = \lim_{\epsilon \to 0} \frac{1}{\Delta A} \langle U^{(1)}(\mathbf{r}'^N) - U^{(0)}(\mathbf{r}^N) \rangle_0, \tag{12}$$

where 0 and 1 are the states previously defined for TA. Unlike Eq. (5) this expression does not involve any exponential functions. This means that we can rigorously attribute to the working expression of γ_{TA2} a corresponding LRC contribution. This was not the case for the original version of TA. Establishing the LRC part of the original TA expression required assuming no dependency between the averages of two exponential terms containing the intrinsic part and the LRC part. This discussion was described in detail elsewhere [20].

However, as expected from a numerical viewpoint, we check that in the case of infinitesimal variations of the surface, the exponential and the logarithm of Eq. (5) can be expanded, leading to equivalence between expressions (5) and (12). The working expression of Eq. (12), $\partial U(\mathbf{r}^N)/\partial A$, which can also be considered as an approximate expression of Eq. (5), results from a rigorous demonstration based upon statistical thermodynamics. In the next section, the different steps leading to the working expressions of γ from the virial route are investigated in the case of particles bearing Lennard-Jones centers and electrostatic charges.

B. Derivation of the potential with respect to the surface

Consider a system with a volume $V = L_x L_y L_z$ composed of N molecules; each of these N molecules with center of mass $\mathbf{r}_i$ contains n_i charges q_{ia} and n_i atoms at position $\mathbf{r}_{ia}$. The configurational energy of this system is

$$U = \sum_{i}^{N-1} \sum_{j=i+1}^{N} \sum_{a=1}^{n_i} \sum_{b=1}^{n_j} u(r_{iajb}) \tag{13}$$

$$= U_{\mathrm{LJ}} + U_{\mathrm{elec}}, \tag{14}$$

where r_{iajb} defined as $\mathbf{r}_{ia} - \mathbf{r}_{jb}$ is the distance between atom a in molecule i and atom b in molecule j. U_{LJ} is the sum of the different pair potentials calculated using the 6-12 Lennard-Jones potential and U_{elec} represents the sum of all electrostatic interactions in the system. The total electrostatic contribution calculated using the Ewald summation method [32,33] for a box with orthogonal axis is written as

$$\begin{aligned} U_{\mathrm{elec}} = & \frac{1}{2\epsilon_0 V} \sum_{k \neq 0} Q(h) S(\mathbf{h}) S(-\mathbf{h}) \\ & + \frac{1}{8\pi\epsilon_0} \sum_i \sum_a \sum_{j \neq i} q_{ia} \sum_b q_{jb} \, \mathrm{erfc}(\alpha r_{iajb}/r_{iajb}) \\ & - \frac{\alpha}{4\pi^{3/2}\epsilon_0} \sum_i \sum_a q_{ia}^2 \\ & - \frac{1}{8\pi\epsilon_0} \sum_i \sum_a \sum_{b \neq a} \frac{q_{ia} q_{ib}}{r_{iaib}} \mathrm{erf}(\alpha r_{iaib}), \end{aligned} \tag{15}$$

where $\mathrm{erfc}(x)$ is the complementary error function and $\mathrm{erf}(x)$ is the error function. α is chosen so that only pair interactions in the central cell need to be considered in evaluating the second term in Eq. (15). The functions $S(\mathbf{h})$ and $Q(h)$ are defined using Eqs. (16) and (17), respectively,

$$S(\mathbf{h}) = \sum_i \sum_a q_{ia} \exp(i\mathbf{h} \cdot \mathbf{r}_{ia}), \tag{16}$$

$$Q(h) = \frac{1}{h^2} \exp\left(- \frac{h^2}{4\alpha^2} \right), \tag{17}$$

where the reciprocal lattice vector $\mathbf{h}$ is defined as $\mathbf{h} = 2\pi(l/L_x, m/L_y, n/L_z)$, where l, m, n take values of $0, \pm 1, \pm 2, \ldots, \pm \infty$. Let us recall that the excluded atoms b of an atom a are atoms that are linked through a bond, angle, or torsion to atom a. The fourth term in Eq. (15) indicates that the summations run only over the excluded atoms b of atom a in the molecule i.

The equations given below were derived by following the same procedure as Davis [30]. For completeness, these equations are proposed here in the case of molecular systems where Lennard-Jones and electrostatic energy contributions are involved. Differentiating the total energy U with respect to the surface A amounts to calculating a certain number of derivatives with respect to A, such as $\partial Q(h)/\partial A$, $\partial S(\mathbf{h})/\partial A$, $\partial Q(-h)/\partial A$, $\partial(\mathbf{h})/\partial A$, and $\partial r_{ij}/\partial A$. To do so, we recall some definitions of important parameters. Let us introduce a new parameter $\mathbf{d}_{ia}$ describing the location of the atom a relative to the center of mass of molecule i. See the Appendix for details about the expressions of the partition function and of its derivative in the new set of scaled coordinates:

$$\mathbf{d}_{ia} = \mathbf{r}_{ia} - \mathbf{r}_i. \tag{18}$$

From the previous equation, we can write

$$\mathbf{d}_{iajb} = \mathbf{r}_{iajb} - \mathbf{r}_{ij}. \tag{19}$$

The scaled coordinates $(\mathbf{s}_{ia})_\alpha$ are defined by $(\mathbf{r}_{ia})_\alpha = (L)_\alpha (\mathbf{s}_{ia})_\alpha$ where α represents the x, y, or z dimension,

$$(\mathbf{r}_{ij})_\alpha = -(\mathbf{d}_{iajb})_\alpha + (\mathbf{s}_{iajb})_\alpha L_\alpha. \tag{20}$$

As $(\mathbf{d}_{iajb})_\alpha$ and $(\mathbf{s}_{iajb})_\alpha$ do not depend upon A, the derivative of $(\mathbf{r}_{ij})_\alpha$ with respect to A becomes

$$\frac{\partial(\mathbf{r}_{ij})_\alpha}{\partial A} = (\mathbf{s}_{iajb})_\alpha \frac{\partial L_\alpha}{\partial A} = \frac{(\mathbf{r}_{iajb})_\alpha}{L_\alpha}\frac{\partial L_\alpha}{\partial A}. \tag{21}$$

The derivative of $\mathbf{r}_{ij}$ with respect to A is

$$\frac{\partial \mathbf{r}_{ij}}{\partial A} = \frac{1}{r_{ij}}\sum_k^{x,y,z} (\mathbf{r}_{ij})_k \left(\frac{\partial(\mathbf{r}_{ij})_k}{\partial A}\right) = \frac{1}{r_{ij}}\sum_k^{x,y,z} (\mathbf{r}_{ij})_k \left(\frac{(\mathbf{r}_{iajb})_k}{L_k}\frac{\partial L_k}{\partial A}\right) \tag{22}$$

and the derivatives of $(\mathbf{h})_\alpha$ and $(\mathbf{h}^2)_\alpha$ with respect to A are given by the following equations:

$$\frac{\partial(\mathbf{h})_\alpha}{\partial A} = \left(-\frac{2\pi l}{(L_\alpha)^2}\frac{\partial L_\alpha}{\partial A}\right), \tag{23}$$

$$\frac{\partial(\mathbf{h}^2)_\alpha}{\partial A} = \left(-\frac{8\pi^2 l^2}{(L_\alpha)^3}\frac{\partial L_\alpha}{\partial A}\right). \tag{24}$$

These expressions require expressing the derivative of the box dimension with respect to the surface. Each component can be written as a function of the overall interfacial area A such as $L_x = A/(2L_y)$, $L_y = A/(2L_x)$, and $L_z = 2V/A$. If $L_x = L_y$, we obtain the following expressions for the derivatives of the box dimensions with respect to the surface area:

$$\frac{\partial L_x}{\partial A} = \frac{1}{2}\left(\frac{A}{2}\right)^{-1/2}\frac{1}{2} = \frac{1}{4L_x}, \tag{25}$$

$$\frac{\partial L_y}{\partial A} = \frac{1}{4L_y}, \tag{26}$$

$$\frac{\partial L_z}{\partial A} = -\frac{2V}{A^2} = -\frac{L_z}{A}. \tag{27}$$

The operational expression of the surface tension γ_{KBZ} is then given by

$$\gamma_{\mathrm{KBZ}} = \left\langle \frac{\partial U}{\partial A} \right\rangle \tag{28}$$

$$\begin{aligned}
&= \frac{1}{4\pi\epsilon_0}\sum_i\sum_a\sum_{j>i}\sum_b -q_{ia}q_{jb}\frac{1}{r_{iajb}}A(\mathbf{r}_{iajb},\mathbf{r}_{ij})\left(\frac{2\alpha}{\sqrt{\pi}r_{iajb}}\exp[-(\alpha^2 r_{iajb}^2)] + \frac{\mathrm{erfc}(\alpha r_{iajb})}{r_{iajb}^2}\right) \\
&+ \frac{1}{V\epsilon_0}\sum_{h\neq 0} Q(h)\mathrm{Im}\left\{\left[\sum_i\sum_a\left(-(\mathbf{r}_{ia})_x\frac{\pi l}{2(L_x)^3} - (\mathbf{r}_{ia})_y\frac{\pi m}{2(L_y)^3} + (\mathbf{r}_{ia})_z\frac{\pi n}{L_xL_yL_z}\right) + A(\mathbf{h},\mathbf{r}_{ia})\exp(-i\mathbf{h}\cdot\mathbf{r}_{ia})\right]\right. \\
&\left.\times\left(\sum_i\sum_a\exp(i\mathbf{h}\cdot\mathbf{r}_{ia})\right)\right\} + \frac{1}{2V}\sum_{h\neq 0}\left(\frac{2\pi^2 l^2}{(L_x)^4} + \frac{2\pi^2 m^2}{(L_y)^4} - \frac{4\pi^2 n^2}{L_xL_y(L_z)^2}\right)\frac{1}{h^4}\exp\left(-\frac{h^2}{4\alpha^2}\right)\left(\frac{h^2}{4\alpha^2}+1\right)S(\mathbf{h})S(-\mathbf{h}) \\
&- \sum_i\sum_a\sum_{j>i}\sum_b\frac{1}{r_{iajb}}A(\mathbf{r}_{iajb},\mathbf{r}_{ij})\frac{48\epsilon_{ij}}{r_{iajb}}\left[\left(\frac{\sigma_{ij}}{r_{iajb}}\right)^{12} - \frac{1}{2}\left(\frac{\sigma_{ij}}{r_{iajb}}\right)^6\right]
\end{aligned} \tag{29}$$

where the function $A(\mathbf{u},\mathbf{v})$ is defined as

$$A(\mathbf{u},\mathbf{v}) = \left((\mathbf{u})_x\frac{(\mathbf{v})_x}{4L_x^2} + (\mathbf{u})_y\frac{(\mathbf{v})_y}{4L_y^2} - (\mathbf{u})_z\frac{(\mathbf{v})_z}{2L_yL_x}\right) \tag{30}$$

Equation (28) is the operational equation of the well-known expression of Kirkwood and Buff [15–18,30] given in the case of electrostatic interactions treated using the conventional three-dimensional (3D) Ewald summation. The route investigated for recovering this expression is the key for providing both a local surface tension from the virial approach and the corresponding LRC contributions.

C. Local expressions of the surface tension

In the case of a planar surface lying in the x,y plane, the surface tension can be calculated from the integration of the normal and tangential components of the pressure tensor as

$$\gamma_{\mathrm{IK}} = \frac{1}{2}\int_{-L_z/2}^{L_z/2}[p_N(z) - p_T(z)]dz. \tag{31}$$

This definition uses local values of the pressure tensor components which cannot be defined unambiguously. However, the arbitrariness of the surface tension at a planar surface does not affect the value of γ. Using this definition, we can extract a local surface tension $\gamma_{\mathrm{IK}}(z_k)$ defined by $[p_N(z_k)$

$-p_T(z_k)]\delta z$, where δz is the thickness of a slab. The total surface tension γ_{IK} is then the half sum of the local surface tension $\gamma_{IK}(z_k)$. We also established a local version of γ_{TA}, which was directly compared to $\gamma_{IK}(z_k)$ [20]. The resulting operational expression is given by

$$\gamma_{TA}(z_k) = \lim_{\epsilon \to 0} -\frac{k_B T}{\Delta A} \ln \left\langle \exp\left(-\frac{U^{(1)}(z_k, \mathbf{r}'^N) - U^{(0)}(z_k, \mathbf{r}^N)}{k_B T} \right) \right\rangle_{k,0}. \tag{32}$$

$\langle \cdots \rangle_{k,0}$ indicates that the average is carried out over the reference state and the k slabs. $U^{(1)}(z_k, \mathbf{r}'^N)$ and $U^{(0)}(z_k, \mathbf{r}^N)$ are the configurational energies of the slab k in the perturbed and reference states. The ambiguity [9] relies on the part of the interaction energy to be included in the volume V_s of the slab. In this calculation, the definition of Ladd and Woodcok [34] was adopted in this work and two energy contributions have been assigned to the slab centered on z_k: one contribution due to the interaction energy between the molecules within the slab and a second contribution due to the interaction energy of the molecules within the slab with those outside the slab. The energy of the slab at the position z_k is defined as

$$U_{z_k} = \frac{1}{2} \sum_{i=1}^{N} \sum_{j \neq i}^{N} \sum_{a}^{n_i} \sum_{b}^{n_j} H_k(z_i) U_{LJ}(r_{iajb}), \tag{33}$$

where $H_k(z_i)$ is a top-hat function with functional values of

$$H_k(z_i) = \begin{cases} 1 & \text{for } z_k - \dfrac{\delta z}{2} < z_i < z_k + \dfrac{\delta z}{2}, \\ 0 & \text{otherwise.} \end{cases} \tag{34}$$

Using this definition, the following condition is satisfied:

$$\int_V dz_k U_{z_k} = U, \tag{35}$$

where U is the total configurational energy of the simulation box and V its volume.

Writing $\Sigma_k \gamma_{TA}(z_k) = \gamma_{TA}$ amounts to assuming that the energy of the slab at the position z_k is uncorrelated with that of the slab at z_{k+1}. These approximations were validated in a previous paper [20].

The second version of the TA approach (TA2) does not contain any exponential term as opposed to the expressions of Eqs. (5) and (32). This allows us to propose a local version of the surface tension without taking into consideration the lack of correlation of the local energies between the different slabs:

$$\gamma_{TA2} = \left\langle \frac{\partial U(\mathbf{r}^N)}{\partial A} \right\rangle_0 \tag{36}$$

$$= \frac{\int d\mathbf{r}^N \dfrac{\partial U(\mathbf{r}^N)}{\partial A} \exp\left(-\dfrac{U(\mathbf{r}^N)}{k_B T} \right)}{\int d\mathbf{r}^N \exp\left(-\dfrac{U(\mathbf{r}^N)}{k_B T} \right)} = \frac{\int d\mathbf{r}^N \dfrac{\partial \sum_k U(z_k, \mathbf{r}^N)}{\partial A} \exp\left(-\dfrac{U(\mathbf{r}^N)}{k_B T} \right)}{\int d\mathbf{r}^N \exp\left(-\dfrac{U(\mathbf{r}^N)}{k_B T} \right)} = \sum_k \frac{\int d\mathbf{r}^N \dfrac{\partial U(z_k, \mathbf{r}^N)}{\partial A} \exp\left(-\dfrac{U(\mathbf{r}^N)}{k_B T} \right)}{\int d\mathbf{r}^N \exp\left(-\dfrac{U(\mathbf{r}^N)}{k_B T} \right)} = \sum_k \gamma_{TA2}(z_k). \tag{37}$$

The calculation of the local value $\gamma_{TA2}(z_k)$ allows a check of the methodology used and can be compared directly to the local value calculated from the Irving-Kirkwood definition $[p_N(z_k) - p_T(z_k)]\delta z$:

$$\gamma_{TA2}(z_k) = \frac{\int d\mathbf{r}^N \dfrac{\partial U(z_k, \mathbf{r}^N)}{\partial A} \exp\left(-\dfrac{U(\mathbf{r}^N)}{k_B T} \right)}{\int d\mathbf{r}^N \exp\left(-\dfrac{U(\mathbf{r}^N)}{k_B T} \right)} = \left\langle \frac{\partial U(z_k, \mathbf{r}^N)}{\partial A} \right\rangle_0. \tag{38}$$

Equation (38) gives explicitly the local version of the TA2 approach. This expression does not require any assumption concerning the absence of correlations between local energetic properties of consecutive slabs. The local version associated with the virial approach is then given by

$$\frac{\partial U}{\partial A} = \sum_k \frac{\partial U_{z_k}}{\partial A}, \tag{39}$$

where $\partial U_{z_k} / \partial A$ is expressed by

$$\gamma_{\mathrm{KBZ}}(z_k) = \frac{\partial U_{z_k}}{\partial A} \tag{40}$$

$$= \sum_{i\in k}\sum_{a}\left(\frac{1}{4\pi\epsilon_0}\sum_{j\neq i}\sum_{b} - q_{ia}q_{jb}\frac{1}{r_{iajb}}A(\mathbf{r}_{iajb},\mathbf{r}_{ij})\left(\frac{2\alpha}{\sqrt{\pi}r_{iajb}}\exp[-(\alpha^2 r_{iajb}^2)] + \frac{\mathrm{erfc}(\alpha r_{iajb})}{r_{iajb}^2}\right)\right.$$
$$+ \frac{1}{V\epsilon_0}\sum_{h\neq 0} Q(h)\mathrm{Im}\left\{\left[\sum_i\sum_a\left(-(\mathbf{r}_{ia})_x\frac{\pi l}{2(L_x)^3} - (\mathbf{r}_{ia})_y\frac{\pi m}{2(L_y)^3} + (\mathbf{r}_{ia})_z\frac{\pi n}{L_xL_yL_z}\right) + A(\mathbf{h},\mathbf{r}_{ia})\exp(-i\mathbf{h}\cdot\mathbf{r}_{ia})\right]\right.$$
$$\left.\left.\times\left(\sum_i\sum_a\exp(i\mathbf{h}\cdot\mathbf{r}_{ia})\right)\right\} + \frac{1}{2V}\sum_{h\neq 0}\left(\frac{2\pi^2 l^2}{(L_x)^4} + \frac{2\pi^2 m^2}{(L_y)^4} - \frac{4\pi^2 n^2}{L_xL_y(L_z)^2}\right)\frac{1}{h^4}\exp\left(-\frac{h^2}{4\alpha^2}\right)\left(\frac{h^2}{4\alpha^2}+1\right)S(\mathbf{h})S(-\mathbf{h})\right.$$
$$\left.- \sum_{j\neq i}\sum_b\frac{1}{r_{iajb}}A(\mathbf{r}_{iajb},\mathbf{r}_{ij})\frac{48\epsilon_{ij}}{r_{iajb}}\left[\left(\frac{\sigma_{ij}}{r_{iajb}}\right)^{12} - \frac{1}{2}\left(\frac{\sigma_{ij}}{r_{iajb}}\right)^6\right]\right) \tag{41}$$

where the center of mass of molecule i is within the slab k. These local versions $\gamma_{\mathrm{TA}}(z_k)$ and $\gamma_{\mathrm{KBZ}}(z_k)$ are directly comparable to the standard local version $\gamma_{\mathrm{IK}}(z_k)$.

D. Long-range corrections to the surface tension

We showed in previous papers [2,20,35] that the value of the surface tension calculated from molecular simulations became independent of the cutoff radius once the long-range corrections were included. Different correction schemes [4–6,8,20] were adopted to take into account the truncation of the dispersion-repulsion interactions on the surface tension. In the case of aqueous solutions, the electrostatic energy contributions are several orders of magnitude higher than the repulsion-dispersion energy contributions; it results from this that the surface tension is not affected by the LRC contributions due to the truncated Lennard-Jones potential. For most other polar liquids, where the different types of interactions are comparable in magnitude, the way of correcting the surface tension becomes crucial. In the case of the simulation of n-alkanes, the inclusion of the LRC contributions is necessary, and such contributions can represent up to 30% of the total value of the surface tension [35].

The expression derived by Blokhuis *et al.* is based on the assumptions that the radial distribution function equals unity beyond the cutoff radius and that the density profile can be represented by a hyperbolic tangent function. This method provides a scalar surface tension and is added after the simulation run. This expression has often been used in conjunction with the Kirkwood-Buff expression. Other approaches [5,6,8,20] are applied in the process of the simulation and give a profile of the LRC contributions to the surface tension along the direction normal to the interface. Slight differences may appear between the different expressions [35]. However, it has been shown [20,35] that the total surface tension was independent of the type of calculation once the appropriate LRC contributions were included in the calculation of the intrinsic contribution. Here, we aim to calculate the LRC profile contribution to γ resulting from the virial approach. The calculation of the intrinsic part of the surface tension with the KBZ approach uses the derivative of the potential with respect to the surface area. It results from this that the calculation of the long-range corrections to the surface tension calculated with the KBZ method must use the derivative of the configurational energy with respect to A. Since the LRC contributions of the normal and tangential components of the pressure tensor used in the IK approach are based upon the method of Guo and Lu, we establish the LRC expressions of the KBZ approach by using the same scheme [6]. Other methods are possible, like the method derived by Janecek [8], for example. The methodology used here can be straightforwardly applied in the case of different LRC contributions. Let us recall the two parts of the LRC contributions to the configurational energy derived by Guo and Lu:

$$U_{\mathrm{LRC}}(z_k) = U_{\mathrm{LRC}}^{(1)}(z_k) + U_{\mathrm{LRC}}^{(2)}(z_k)$$
$$= 2\pi\rho^2(z_k)V_s\int_{r_c}^{\infty}dr\int_{-r}^{r}d\Delta z\; rU_{\mathrm{LJ},m}(r)$$
$$+ \pi\rho(z_k)V_s\int_{r_c}^{\infty}dr\int_{-r}^{r}d\Delta z\sum_{i=1}^{N_s}[\rho(z_{k+i})$$
$$- \rho(z_{k+i-1})]rU_{\mathrm{LJ},m}(r), \tag{42}$$

where $U_{\mathrm{LJ},m}(r)$ is defined by

$$U_{\mathrm{LJ},m}(r) = \sum_{a=1}^{N_a}\sum_{b=1}^{N_b}4\epsilon_{ab}\left[\left(\frac{\sigma_{ab}}{r}\right)^{12} - \left(\frac{\sigma_{ab}}{r}\right)^6\right]. \tag{43}$$

Δz is the difference $(z-z_k)$ and varies between $-r$ and r. N_s is the number of slabs between z_k and z. The first term is similar to that used in homogeneous systems except for the use of a density $\rho(z_k)$ depending on z_k. The second term takes into account the fact that each slab z_k is surrounded by slabs of different local densities.

Differentiating, at constant volume, the LRC parts of the configurational energy with respect to A amounts to considering the following derivative expression:

$$\frac{\partial U_{\mathrm{LRC}}(z_k)}{\partial A} = 2\pi\rho^2(z_k)V_s\int_{r_c}^{\infty} dr\int_{-r}^{r} d\Delta z\left(\frac{\partial r}{\partial A}U_{\mathrm{LJ},m}(r) + r\frac{\partial U_{\mathrm{LJ},m}(r)}{\partial A}\right) + \pi\rho(z_k)V_s\int_{r_c}^{\infty} dr\int_{-r}^{r} d\Delta z[\rho(z) - \rho(z_k)]\left(\frac{\partial r}{\partial A}U_{\mathrm{LJ},m}(r) + r\frac{\partial U_{\mathrm{LJ},m}(r)}{\partial A}\right)$$

$$= 2\pi\rho^2(z_k)V_s\int_{r_c}^{\infty} dr\int_{-r}^{r} d\Delta z\frac{\partial r}{\partial A}\left(U_{\mathrm{LJ},m}(r) + r\frac{\partial U_{\mathrm{LJ},m}(r)}{\partial r}\right) + \pi\rho(z_k)V_s\int_{r_c}^{\infty} dr\int_{-r}^{r} d\Delta z[\rho(z) - \rho(z_k)]\frac{\partial r}{\partial A}\left(U_{\mathrm{LJ},m}(r) + r\frac{\partial U_{\mathrm{LJ},m}(r)}{\partial r}\right). \quad (44)$$

Using Eq. (22), the derivative of r with respect to A can be written as

$$\frac{\partial r}{\partial A} = \frac{1}{r}\left(\frac{(\mathbf{r})_x^2}{4L_x^2} + \frac{(\mathbf{r})_y^2}{4L_y^2} - \frac{(\mathbf{r})_z^2}{A}\right) = \frac{1}{2rA}[r^2 - 3(\mathbf{r})_z^2]. \quad (45)$$

By using the fact that $(\mathbf{r})_z$ corresponds to Δz, Eq. (44) becomes

$$\frac{\partial U_{\mathrm{LRC}}(z_k)}{\partial A} = 2\pi\frac{V_s}{2A}\rho^2(z_k)\int_{r_c}^{\infty} dr\int_{-r}^{r} d\Delta z\left(\frac{r^2 - 3(\Delta z)^2}{r}\right)\times\left(U_{\mathrm{LJ}}(r) + r\frac{\partial U_{\mathrm{LJ},m}(r)}{\partial r}\right) + \pi\rho(z_k)\frac{V_s}{2A}\int_{r_c}^{\infty} dr\int_{-r}^{r} d\Delta z[\rho(z) - \rho(z_k)]\times\left(\frac{r^2 - 3(\Delta z)^2}{r}\right)\left(U_{\mathrm{LJ},m}(r) + r\frac{\partial U_{\mathrm{LJ},m}(r)}{\partial r}\right). \quad (46)$$

The integration of the first term of Eq. (46) results in a zero value, and the operational expression of the LRC contribution to the surface tension calculated through the KBZ approach becomes

$$\gamma_{\mathrm{KBZ,LRC}}(z_k) = \pi\rho(z_k)\frac{V_s}{2A}\int_{r_c}^{\infty} dr\int_{-r}^{r} d\Delta z[\rho(z) - \rho(z_k)]\times\left(\frac{r^2 - 3(\Delta z)^2}{r}\right)\left(U_{\mathrm{LJ},m}(r) + r\frac{\partial U_{\mathrm{LJ},m}(r)}{\partial r}\right). \quad (47)$$

The LRC contribution relative to the second version of the TA method is expressed using the difference between the LRC terms of the configurational energy in the perturbed and reference states:

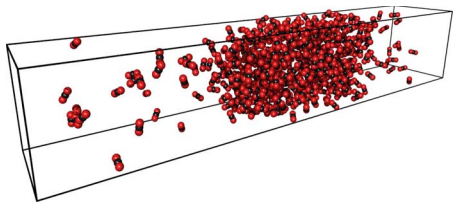

FIG. 2. (Color online) Typical configuration of a carbon dioxide liquid-vapor interface at $T=228$ K. Carbon atoms are represented in black while oxygen atoms are in red.

$$\gamma_{\mathrm{TA2,LRC}}(z_k) = \lim_{\epsilon\to 0}\frac{1}{\Delta A}[U_{\mathrm{LRC}}(z_k') - U_{\mathrm{LRC}}(z_k)] \quad (48)$$

$$= \lim_{\epsilon\to 0}\frac{1}{\Delta A}[U_{\mathrm{LRC}}^{(2)}(z_k') - U_{\mathrm{LRC}}^{(2)}(z_k)], \quad (49)$$

where $U_{\mathrm{LRC}}(z_k')$ and $U_{\mathrm{LRC}}(z_k)$ are the LRC configurational energies of the perturbed and reference states, respectively. Whereas the difference between the first terms $U_{\mathrm{LRC}}^{(1)}(z_k')$ and $U_{\mathrm{LRC}}^{(1)}(z_k)$ cancels because the perturbation process conserves the local density in the two states, the second term depends on $d\Delta z$ and is changed by the transformation. The operational expression given by Eq. (49) does not require any assumption about the lack of correlation between the LRC part and the intrinsic part as was the case in the TA method [20].

The other expressions for the LRC contributions to the surface tensions $\gamma_{\mathrm{IK,LRC}}$ and $\gamma_{\mathrm{KB,LRC}}$ are given elsewhere [20,35].

III. RESULTS AND DISCUSSION

The simulation box is a rectangular parallelepiped box of dimensions $L_xL_yL_z$ ($L_x=L_y$) with N n-pentane, CO_2, or H_2O molecules (see Fig. 2). The details of the geometry of the system and the total number of molecules are given in Table I. We can use periodic boundary conditions either in three dimensions or only in the x and y directions. In the latter case, the system has a finite length along the direction perpendicular to the surface and two hard reflecting walls must be added. The three-dimensionally periodic system allows

TABLE I. Dimensions of the simulation box, temperature, number of molecules and relative probabilities for the different types of MC moves.

	n-pentane	CO_2	H_2O
$L_x=L_y$ (Å)	35	25	20
L_z (Å)	235	151	100
N	500	512	500
T (K)	300	228	388
% (translation)	45	50	50
% (rotation)	35	50	50
% (internal)	20	0	0

the use of the conventional Ewald summation [32,33] for the treatment of the electrostatic interactions and the number of reciprocal lattice vectors must be consistent with the box dimensions. An excellent discussion about the use of the conventional Ewald summation for the simulation of a two-phase system is given by Alejandre [31]. In the case of systems that are periodic in two dimensions, a two-dimensional technique [36–39] must be applied. However, it is well known that the Ewald quasi-2D method is much more expensive than the 3D Ewald summation. Therefore, the first solution consisting in applying the periodic boundary condition in all directions and using the 3D Ewald summation technique has been adopted in this work as is the case of most simulations of two-phase systems.

Monte Carlo (MC) simulations were performed in the *NVT* ensemble. Each cycle consisted of N randomly selected moves with fixed probabilities. The moves were (1) displacement of the center of mass of a random molecule, (2) rotation of a randomly selected molecule around its center of mass, and (3) regrowth of part of a random molecule using the configurational-bias scheme [40] in the case of flexible molecules. The relative probabilities for the different moves are given in Table I for each studied molecule. The second contribution of the LRCs to the configurational energy of Eq. (42) consisted in a double integral which contains a series of density differences that render this part cumbersome to calculate. Concerning this term, it was shown [35] that it represented only a minor contribution of the total long-range energy. As a consequence, only the first part of the long-range correction energy was included here in the total configurational energy. The total long-range correction energy U_{LRC} was calculated by summing up all the local contributions of each slab and was calculated after each move of molecular position. The U_{LRC} term was then added to the total energy of the system to be used in the Metropolis scheme.

The initial configuration was built by placing N molecules on the nodes of a fcc lattice included in a cubic box with random orientations. MC simulations in the *NpT* ensemble were performed on this bulk fluid configuration. The dimensions of the resulting configurations were increased along the z axis by placing two empty cells on both sides of the bulk liquid box. A typical MC run consisted of 100 000 cycles for equilibration and 200 000 cycles for the production phase. The surface tension was calculated every ten cycles. The statistical errors for these properties were estimated using ten block averages of 2000 configurations. As the geometry of the system shows a heterogeneity along the axis normal to the interface (z axis), a dependence of the thermodynamic properties is expected only in this direction. We calculated the local surface tension and its long-range correction as a function of z_k by splitting the cell into slabs of width δz.

The n-pentane molecule was modeled using the anisotropic united atom (AUA-4) force field [41]. Within this model, the force centers are located on the external bisector of the angle formed by neighboring bonds. The intermolecular interactions were modeled using the 6-12 Lennard-Jones potential. We used the same potential energy to describe the nonbonded interactions between atoms separated by more than three bonds in n-pentane. The unlike interatomic interactions were calculated using the Lorentz-Berthelot combining rules, i.e., a geometric combining rule for the energy and an arithmetic combining rule for the atomic size. In the case of n-pentane, the bond angle interactions were calculated using $U_{\mathrm{bend}}=k_{\mathrm{bend}}/2[\cos(\theta)-\cos(\theta_0)]$ and the torsion potential was given by $U_{\mathrm{tors}}=\Sigma_{n=0}^{8}a_n\cos^n(\phi)$. The different parameters of the AUA-4 model are given in Table II. The CO_2 molecule was described using the rigid version of the Harris and Yung potential [42] with three Lennard-Jones centers and three electrostatic charges (see Table III). The carbon-oxygen bond lengths were fixed and equal to 1.149 Å and the carbon dioxide molecule had a fixed OCO angle of 180°. The water molecule was modeled using the TIP4P-Ew rigid model [43],

TABLE II. n-pentane [41] potential parameters.

n-pentane (AUA4 model)			
	σ (Å)	ϵ (K)	δ (Å)
CH_2	3.4612	86.29	0.38405
CH_3	3.6072	120.15	0.21584
C-C distance (Å)			1.535
Bending			
$C\text{-}CH_2\text{-}C$		θ_0 (deg)	114
		k_{bend} (K)	74900
Torsion			
$C\text{-}CH_2\text{-}CH_2\text{-}C$		a_0 (K)	1001.35
		a_1 (K)	2129.52
		a_2 (K)	−303.06
		a_3 (K)	−3612.27
		a_4 (K)	2226.71
		a_5 (K)	1965.93
		a_6 (K)	−4489.34
		a_7 (K)	−1736.22
		a_8 (K)	2817.37

TABLE III. CO_2 [42] and water [43] potential parameters.

CO_2			
	σ (Å)	ϵ (K)	Charge (e)
C	2.757	28.129	+0.6512
O	3.033	80.507	−0.3256
C=0 distance (Å)			1.149
O=C=0 angle (deg)			180
H_2O (TIP4P-Ew model)			
	σ (Å)	ϵ (K)	Charge (e)
O	3.16435	81.9	0
H	0	0	0.52422
M	0	0	−1.04844
OH distance (Å)			0.9572
H-O-H angle (deg)			104.52
OM distance (Å)			0.1250

TABLE IV. Surface tension contributions (LRC, intrinsic and total) (mN m^{-1}) calculated from different operational expressions in the cases of *n*-pentane (T=300 K), CO_2 (T=228 K), and water (T=388 K) systems. The surface tensions resulting from the TA, TA2, KBZ, and IK methods are calculated from Eqs. (5), (12), (28), and (31), respectively. The operational expression using the Buff method has been given elsewhere [2,20,35]. The experimental surface tensions are reported for comparison (*n*-pentane [49], CO_2 [50], H_2O [51]). The subscripts give the accuracy of the last decimal(s), i.e., $44.0_{6.0}$ means 44.0 ± 6.0.

System	γ_{TA}	γ_{TA2}	γ_{KBZ}	γ_{IK}	γ_{KB}	$\gamma_{Exp.}$
			LRC contributions			
n-pentane	$3.1_{.2}$	$3.1_{.2}$	$3.3_{.3}$	$3.9_{.3}$	$4.9_{.5}$	
CO_2	$2.1_{.1}$	$2.1_{.1}$	$2.4_{.1}$	$3.0_{.1}$	$3.3_{.3}$	
H_2O	$3.0_{.1}$	$3.0_{.1}$	$3.8_{.1}$	$4.5_{.1}$	$5.3_{.3}$	
			Intrinsic part			
n-pentane	$13.2_{1.7}$	$13.2_{1.7}$	$12.0_{1.8}$	$12.0_{1.8}$	$12.0_{1.8}$	
CO_2	$13.4_{2.3}$	$13.4_{2.2}$	$12.1_{2.3}$	$12.1_{2.3}$	$12.1_{2.3}$	
H_2O	$44.0_{6.0}$	$44.0_{6.0}$	$42.9_{6.0}$	$42.9_{6.0}$	$42.9_{6.3}$	
			Total surface tension			
n-pentane	$16.3_{1.9}$	$16.3_{1.9}$	$15.3_{2.1}$	$15.9_{2.1}$	$16.9_{2.2}$	15.2
CO_2	$15.5_{2.4}$	$15.5_{2.3}$	$14.5_{2.4}$	$15.1_{2.4}$	$15.4_{2.7}$	14.3
H_2O	$47.0_{6.1}$	$47.0_{6.1}$	$46.7_{6.1}$	$47.4_{6.1}$	$48.2_{6.6}$	56.0

where the oxygen site contributes only to the LJ term and carries no charge. Ew indicates that the parameters of this model have been established from simulations using the Ewald summation method. This model introduces a bare charge at a new site M, located on the bisector of the HOH bond angle (Table III). This model is a recent reparametrization to take into account the use of the long-range interactions calculated from the Ewald method. Within the CO_2 model, the cross interactions were calculated using the Lorentz-Berthelot rules.

A relatively small cutoff of 12 Å was used in order to bring the two-phase simulations in line with those carried out with the Gibbs ensemble Monte Carlo (GEMC) method [44–46]. In this case, the use of the long-range corrections to be added to the interfacial properties is meaningful. For systems with electrostatic interactions calculated using the Ewald technique, we took $\mathbf{h}_x^{\max}=\mathbf{h}_y^{\max}=8$ and $\mathbf{h}_z^{\max}=35$ to respect both the ratio of the box dimensions and the convergence of the reciprocal space contribution of the surface tension. Concerning the computational CPU time required for the calculation of the surface tension, the TA and KBZ methods are 1.7 and 1.4 times faster than the IK method, respectively.

Using the test-area method, the calculation of the surface tension was carried out in the direct and reverse directions. The calculation of the direct direction involves an increase of the surface area as $A^{(1)}=A^{(0)}+\Delta A_\epsilon$, whereas a decrease of the surface area was performed in the reverse path as $A^{(-1)}=A^{(0)}-\Delta A_\epsilon$. ΔA_ϵ is equal to $L_x^{(0)}L_y^{(0)}\epsilon$ where ϵ is fixed to 5×10^{-4}. The surface tension value was averaged over the two directions as $(\gamma_D-\gamma_R)/2$ where γ_D and γ_R are expressed as

$$-\frac{k_BT}{2\Delta A_\epsilon}\ln\left\langle \exp\left(-\frac{\Delta U_{(0\to1)}}{k_BT}\right)\right\rangle_0$$

and

$$-\frac{k_BT}{2\Delta A_\epsilon}\ln\left\langle \exp\left(-\frac{\Delta U_{(0\to-1)}}{k_BT}\right)\right\rangle_0,$$

respectively. The perturbation of the box dimensions was performed over the configurations of the reference state and led to virtual configurations of the perturbed state. The ensemble average was carried out over the reference system and the virtual configurations of the perturbed system did not participate in the Markov chain of states.

We compared the different operational expressions for the surface tension of three systems: *n*-pentane at T=300 K, carbon dioxide at T=228 K, and water at T=338 K. The long-range corrections and the intrinsic part of the surface tension are reported in Table IV for different surface tension expressions. First, it can be seen that the different expressions predict correctly the surface tension for the *n*-pentane and CO_2 systems with a deviation less than 10% with respect to the experimental value. The agreement remains satisfactory with the water TIP4P-Ew model even though the deviation can reach 15%. The difference between the calculated and experimental values for water must be attributed both to the model and to the truncation procedures. The recent calculations [47] of the surface tension with this TIP4P-Ew model using MD simulations confirm this analysis.

With the KBZ method, the long-range corrections are slightly greater than those obtained from the TA and TA2 approaches and smaller than those derived from the IK and Buff methods. These differences are due to the fact that these expressions are not completely equivalent and result from different approximations. The discrepancies between the different ways of correcting the surface tension decrease in magnitude with larger values of the cutoff radius [35]. The use of a relatively small cutoff value makes essential the use of appropriate LRC contributions within each definition of the surface tension. The intrinsic part of the surface tension

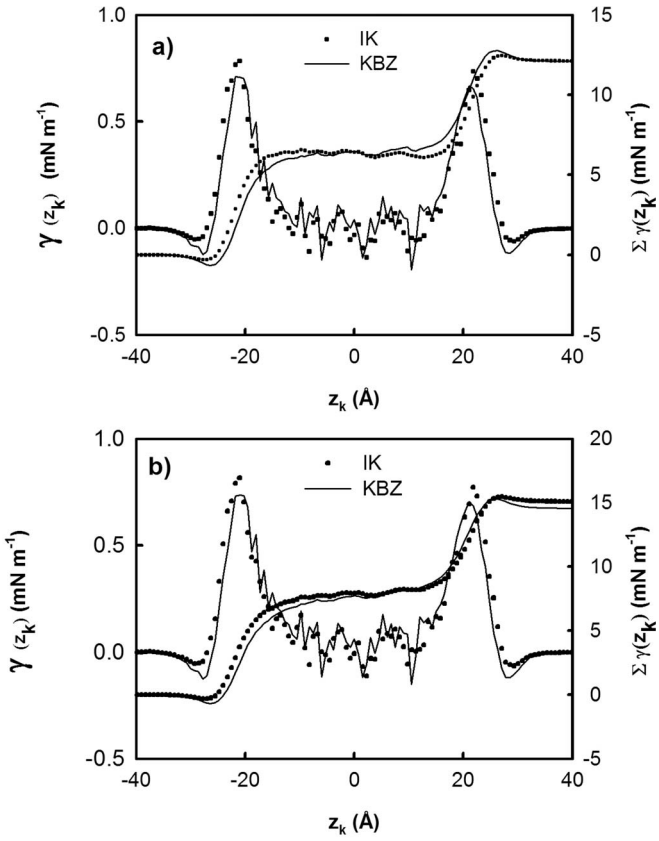

FIG. 3. Surface tension profiles calculated from MC simulations of CO_2 at $T=228$ K using the IK definition and the KBZ approach (left axis) and the corresponding integral curve (right axis). (a) Intrinsic part and (b) total part calculated from the sum of the intrinsic and LRC parts.

calculated from the KBZ method is slightly smaller than that calculated from the perturbation techniques and is close to the value calculated from the mechanical approaches. We check that the present operational expression of the surface tension (KBZ) compares very well with the expressions resulting from the perturbation (TA,TA2) and the mechanical (IK,KB) routes. We also confirm that the approximations made in the previous paper [20] concerning the absence of correlations between the $\langle \exp[-(\Delta U)/k_BT]\rangle$ and $\langle \exp[-\Delta U_{\mathrm{LRC}}/k_BT]\rangle$ terms remains valid because the expression TA2 which requires no approximation gives the same value as that of the TA method within the statistical fluctuations.

Figure 3(a) compares the profiles of the intrinsic local surface tension $\gamma(z_k)$ calculated from the mechanical method (IK) and from the virial route (KBZ) in the case of the CO_2 two-phase system. In a first step, we compare the profile resulting from the KBZ method to that calculated from the IK method because the IK technique has been widely applied for the calculation of the profile of the surface tension in the literature [1,2,11,12,20,35]. The profiles resulting from the two methods present the same features both in the vapor and in the liquid regions. It can be seen that the region close to the surface exhibits a negative peak on the vapor side of the interface in the KBZ calculation. This feature has been the subject of controversial discussions and depends on the method used for the calculation of the pressure tensor [11,48]. The magnitude of these peaks decreases within the Harasima expression [13].

This negative peak has also been observed in the profile obtained with the TA method [20]. Figure 3(a) shows that the local integral of the surface tension profile is constant throughout the liquid and vapor regions, indicating that these two phases have no contribution to the surface tension. It is clear from the profiles that the two interfaces are well defined and symmetric around the middle of the slab, indicating that the contribution from both surfaces is the same. The fact that the integral is constant in the liquid region means that this region does not contribute to the surface tension and indicates that the two interfacial regions are independent with no interaction between them. Figure 3(b) (right axis) shows that the integral of the surface tension tends to the same value for the IK and KBZ methods. It has also been checked that the surface tension calculated from the sum of the local values [Eq. (40)] and from Eq. (28) is identical. Figure 3(b) shows the profiles of the total surface tensions; these profiles present the same features as the profiles of the intrinsic part. The total surface tension calculated from the integral of the local surface tension profile (right axis) matches very well between the KBZ and IK methods.

Figure 4(a) shows the profiles of the total surface tensions calculated from the perturbation approach (TA and TA2) and the KBZ technique. We observe that the profiles cannot be distinguished between the three methods, whereas the integral of the KBZ profile shows a surface tension value slightly smaller than that resulting from TA and TA2 in agreement with the values given in Table IV. Figure 4(b) presents the profiles of the long-range corrections of γ for the different methods. The profiles differ in the magnitudes of the positive peaks, which explains the differences between the different tail corrections given in Table IV.

IV. CONCLUSIONS

We have established an operational expression for the local surface tension calculated from the virial route. This expression constitutes the local version of the well-known expression of Kirkwood and Buff. Additionally, we have given the local version of the long-range corrections of γ within this approach. We have also presented for completeness the local version of the TA approach within the TI approach as opposed to the TA expression calculated from the FEP formalism. In the case of small perturbation of the surface, the expression for γ derived from TI can be seen as an approximate expression of the original version of the TA approach. This reformulated expression takes advantage of providing a LRC expression for the surface tension without needing to assume approximations about the lack of correlations between terms containing the intrinsic and LRC parts. The different operational expressions for the surface tension using both the mechanical and thermodynamical routes have been discussed as applied to the *n*-pentane, carbon dioxide, and water liquid-vapor interfaces. The KBZ method produces values in agreement with the different methods and with the

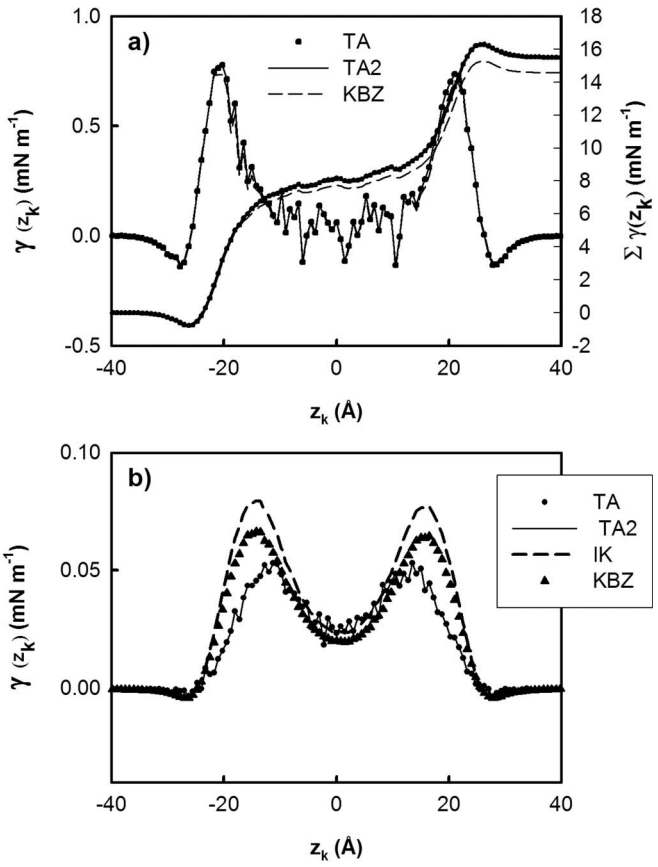

FIG. 4. (a) Total surface tension profiles calculated from MC simulations of CO_2 at $T=228$ K using the TA, TA2, and KBZ methods (left axis) and the corresponding integral curves (right axis) and (b) LRC profiles of the surface tension calculated from the TA, TA2, IK, and KBZ approaches.

experimental values for the studied compounds. In the case of water, a small deviation compared to experiments has been observed. This deviation is mainly attributed to the water model used rather than the methodology employed. Additionally, the KBZ method has the advantage of providing a profile of the surface tension and of being faster than the traditional IK method.

APPENDIX: EXPRESSION FOR THE DERIVATIVE OF THE PARTITION FUNCTION WITH RESPECT TO THE SURFACE AREA IN A SET OF SCALED COORDINATES

In the case of changes of variables like those carried out in Eqs. (18)–(20), we propose to show that the surface tension can be written as $\langle \partial U/\partial A \rangle$. For convenience and clarity, let us consider a planar surface system of N particles in the NVT statistical ensemble. The Q_{NVT} partition function is then expressed as

$$Q_{NVT} = \frac{1}{\Lambda^{3N} N!} \int d\mathbf{r}^N \exp\left(-\frac{U(\mathbf{r}^N)}{k_B T}\right) \tag{A1}$$

$$= \frac{1}{\Lambda^{3N} N!} \int (|J| d\mathbf{s})^N \exp\left(-\frac{U(\mathbf{s}^N)}{k_B T}\right), \tag{A2}$$

where $\mathbf{s}^N$ is a set of coordinates scaled with the dimensions of the simulation cell and defined by $\mathbf{r}^N = L\mathbf{s}^N$ and $|J|$ is the Jacobian of the transformation of Eq. (A3). The $\mathbf{r}^N = L\mathbf{s}^N$ expression is equivalent to that of Eq. (20) for a system of N particles:

$$\int dr_x dr_y dr_z = \int |J| ds_x ds_y ds_z. \tag{A3}$$

The Jacobian $|J|$ contains all the first-order derivatives of the vector $\mathbf{r}$ with respect to $\mathbf{s}$. For a given particle i, the Jacobian $|J_i|$ is written as

$$|J_i| = \begin{vmatrix} \frac{\partial r_x}{\partial s_x} & \frac{\partial r_x}{\partial s_y} & \frac{\partial r_x}{\partial s_z} \\ \frac{\partial r_y}{\partial s_x} & \frac{\partial r_y}{\partial s_y} & \frac{\partial r_y}{\partial s_z} \\ \frac{\partial r_z}{\partial s_x} & \frac{\partial r_z}{\partial s_y} & \frac{\partial r_z}{\partial s_z} \end{vmatrix} = L_x L_y L_z = V.$$

For N particles, the Jacobian $|J|$ becomes equal to V^N and the Q_{NVT} partition function takes the form of the well-known expression [52]

$$Q_{NVT} = \frac{V^N}{\Lambda^{3N} N!} \int d\mathbf{s}^N \exp\left(-\frac{U(\mathbf{s}^N)}{k_B T}\right). \tag{A4}$$

The derivative of the partition function with respect to A leads to consideration of the following derivatives of Eq. (A5):

$$\frac{\partial Q_{NVT}}{\partial A} = \frac{N V^{N-1}}{\Lambda^{3N} N!} \left(\frac{\partial V}{\partial A}\right) \int d\mathbf{s}^N \exp\left(-\frac{U(\mathbf{s}^N)}{k_B T}\right) + \frac{V^N}{\Lambda^{3N} N!} \int d\mathbf{s}^N \frac{1}{k_B T} \left(\frac{\partial U(\mathbf{s}^N)}{\partial A}\right) \exp\left(-\frac{U(\mathbf{s}^N)}{k_B T}\right). \tag{A5}$$

Equation (A5) is related to the density number ρ defined by N/V. Given that the transformation conserves the volume and that the surface is planar, the derivative of the volume with respect to A in Eq. (A5) is zero. The derivative of the partition function with respect to A rewritten in the original set of coordinates $\mathbf{r}^N$ is then expressed by Eq. (A6) which is strictly equivalent to Eq. (9):

$$\frac{\partial Q_{NVT}}{\partial A} = \frac{1}{\Lambda^{3N} N!} \int d\mathbf{r}^N \frac{1}{k_B T} \left(\frac{\partial U(\mathbf{r}^N)}{\partial A}\right) \exp\left(-\frac{U(\mathbf{r}^N)}{k_B T}\right). \tag{A6}$$

[1] A. Trokhymchuk and J. Alejandre, J. Chem. Phys. **111**, 8510 (1999).
[2] F. Goujon, P. Malfreyt, J. M. Simon, A. Boutin, B. Rousseau, and A. H. Fuchs, J. Chem. Phys. **121**, 12559 (2004).
[3] E. Salomons and M. Mareschal, J. Phys.: Condens. Matter **3**, 3645 (1991).
[4] E. M. Blokhuis, D. Bedeaux, C. D. Holcomb, and J. A. Zollweg, Mol. Phys. **85**, 665 (1995).
[5] M. Mecke and J. Winkelmann, J. Chem. Phys. **107**, 9264 (1997).
[6] M. Guo and B. C. Y. Lu, J. Chem. Phys. **106**, 3688 (1997).
[7] M. Mecke, J. Winkelmann, and J. Fischer, J. Chem. Phys. **110**, 1188 (1999).
[8] J. Janecek, J. Phys. Chem. B **110**, 6264 (2006).
[9] J. S. Rowlinson and B. Widom, *Molecular Theory of Capillarity* (Clarendon Press, Oxford, 1982).
[10] J. H. Irving and J. G. Kirkwood, J. Chem. Phys. **18**, 817 (1950).
[11] J. P. R. B. Walton, D. J. Tildesley, and J. S. Rowlinson, Mol. Phys. **48**, 1357 (1983).
[12] J. P. R. B. Walton, D. J. Tildesley, and J. S. Rowlinson, Mol. Phys. **58**, 1013 (1986).
[13] A. Harasim, Adv. Chem. Phys. **1**, 203 (1957).
[14] P. Schofield and J. R. Henderson, Proc. R. Soc. London, Ser. A **379**, 231 (1982).
[15] J. G. Kirkwood and F. P. Buff, J. Chem. Phys. **17**, 338 (1949).
[16] F. B. Buff, Z. Elektrochem. **56**, 311 (1952).
[17] A. G. McLellan, Proc. R. Soc. London, Ser. A **213**, 274 (1952).
[18] A. G. McLellan, Proc. R. Soc. London, Ser. A **217**, 92 (1953).
[19] G. J. Gloor, G. J. Jackson, F. J. Blas, and E. Miguel, J. Chem. Phys. **123**, 134703 (2005).
[20] C. Ibergay, A. Ghoufi, F. Goujon, P. Ungerer, A. Boutin, B. Rousseau, and P. Malfreyt, Phys. Rev. E **75**, 051602 (2007).
[21] R. W. Zwanzig, J. Chem. Phys. **22**, 1420 (1954).
[22] G. M. Torrie and J. P. Valleau, Chem. Phys. Lett. **28**, 578 (1974).
[23] M. Mezei and D. L. Beveridge, Ann. N.Y. Acad. Sci. **482**, 1 (1986).
[24] J. G. Kirkwood, J. Chem. Phys. **3**, 300 (1935).
[25] D. A. Pearlman, J. Comput. Chem. **15**, 105 (1994).
[26] M. Mezei, S. Swaminathan, and D. L. Beveridge, J. Am. Chem. Soc. **100**, 3255 (1978).
[27] S. M. Thompson, K. E. Gubbins, J. P. R. B. Walton, R. A. R. Chantry, and J. S. Rowlinson, J. Chem. Phys. **81**, 530 (1984).
[28] M. Baus and H. El Bardouni, J. Non-Equilib. Thermodyn. **25**, 229 (2001).
[29] M. Mareschal, M. Baus, and R. Lowett, J. Chem. Phys. **106**, 645 (1997).
[30] H. T. Davis, J. Chem. Phys. **62**, 3412 (1975).
[31] J. Alejandre and D. J. Tildesley, J. Chem. Phys. **102**, 4574 (1995).
[32] M. P. Allen and D. J. Tildesley, *Computer Simulation of Liquids* (Clarendon Press, Oxford, 1987).
[33] E. R. Smith, Proc. R. Soc. London, Ser. A **375**, 475 (1981).
[34] A. J. C. Ladd and L. V. Woodcok, Mol. Phys. **36**, 611 (1978).
[35] F. Goujon, P. Malfreyt, A. Boutin, B. Rousseau, and A. H. Fuchs, J. Chem. Phys. **116**, 8106 (2002).
[36] D. E. Parry, Surf. Sci. **49**, 433 (1975).
[37] S. W. De Leeuw and J. W. Perram, Mol. Phys. **37**, 1313 (1979).
[38] J. Hautman and M. L. Klein, Mol. Phys. **75**, 379 (1992).
[39] J. Lekner, Physica A **157**, 826 (1989).
[40] B. Smit, S. Karaborni, and J. L. Siepmann, J. Chem. Phys. **102**, 2126 (1995).
[41] P. Ungerer, C. Beauvais, J. Delhommelle, A. Boutin, B. Rousseau, and A. H. Fuchs, J. Chem. Phys. **112**, 5499 (2000).
[42] J. Harris and K. Yung, J. Phys. Chem. **99**, 12021 (1995).
[43] H. W. Horn, W. C. Swope, J. W. Pitera, J. D. Madura, T. J. Dick, G. L. Hura, and T. Head-Gordon, J. Chem. Phys. **120**, 9665 (2004).
[44] A. Z. Panagiotopoulos, Mol. Phys. **61**, 813 (1987).
[45] A. Z. Panagiotopoulos, N. Quirke, M. Stapleton, and D. J. Tildesley, Mol. Phys. **63**, 527 (1988).
[46] A. Z. Panagiotopoulos, Mol. Simul. **9**, 1 (1992).
[47] C. Vega and E. de Miguel, J. Chem. Phys. **126**, 154707 (2007).
[48] H. T. Davis and L. E. Scriven, Adv. Chem. Phys. **49**, 357 (1982).
[49] J. Gmehling, CODATA Bull. **58**, 56 (1985).
[50] Data taken from the saturation properties of carbon dioxide at http://webbook.nist.gov.
[51] J. J. Jasper, J. Phys. Chem. Ref. Data **1**, 841 (1972).
[52] D. Frenkel and B. Smit, *Understanding Molecular Simulation*, 2nd ed. (Academic Press, New York, 2002).